ADVANCED FUNCTIONAL MATERIALS
www.afm-journal.de

Topology Optimization-Based Inverse Design of Plasmonic Nanodimer with Maximum Near-Field Enhancement

Yiqin Chen, Yueqiang Hu, Jingyi Zhao, Yunsheng Deng, Zhaolong Wang, Xing Cheng, Dangyuan Lei, Yongbo Deng,* and Huigao Duan**

The near-field enhancement factor is one of the most significant parameters to evaluate the performance of plasmonic nanostructures. Numerous efforts have been made to maximize the enhancement factor through optimizing the size, shape, and spatial arrangement of metallic nanostructures with simple geometries, such as disk, triangle, and rod. This work implements topology optimization to inversely design a metallic nanoparticle dimer with the goal of optimizing the near-field enhancement factor in its sub-10 nm gap. By optimizing the material layout within a given design space, the topology optimization algorithm results in a plasmonic nanodimer of two heart-shaped particles having both convex and concave features. Full-wave electromagnetic analysis reveals that the largest near-field enhancement in the heart-shaped nanoparticle dimer is originated from the greatest concentration of surface charges at the nano-heart apex. Inversely designed heart-, bowtie-, and disk-shaped nanodimers are fabricated by using focused helium ion beam milling with a "sketch and peel" strategy, and their near-field enhancement performances are characterized with nonlinear optical spectroscopies at the single-particle level. Indeed, the heart-shaped nanodimer exhibits much stronger signal intensities than the other two structures. The present work corroborates the validity and effectiveness of topology optimization-based inverse design in achieving desired plasmonic functionalities.

1. Introduction

The giant near-field enhancement associated with plasmon resonances reinforces the interaction of light with matters located in or nearby a metallic nanostructure. The field enhancement factor is one of the most important parameters quantifying the performance of plasmonic nanostructures and determines the efficiencies of many plasmon-amplified radiative and nonradiative linear and nonlinear optical processes, such as plasmon-enhanced fluorescence,[1,2] photoluminescence,[3–5] surface-enhanced Raman scattering,[6–8] optical harmonic generation,[9–12] hot-carrier generation,[13–15] sub-bandgap photodetection,[16,17] and plasmonic local heating-assisted magnetic recording.[18–20] Hence, achieving the maximal possible near-field enhancement in metallic nanostructures has been a long-lasting topic in the field of plasmonics.

Compared to that of isolated plasmonic nanoparticles, the near-field enhancement factors in nanoparticle dimers or

Dr. Y. Chen, Dr. Y. Hu, Dr. Z. Wang, Prof. H. Duan
State-Key Laboratory of Advanced Design and Manufacturing for Vehicle Body
College of Mechanical and Vehicle Engineering
Hunan University
Changsha 410082, China
E-mail: duanhg@hnu.edu.cn

J. Zhao
State Key Laboratory for Mesoscopic Physics & Collaborative Innovation Center of Quantum Matter
Department of Physics
Peking University
Beijing 100871, China

J. Zhao
Department of Applied Physics
The Hong Kong Polytechnic University
Hong Kong, China

The ORCID identification number(s) for the author(s) of this article can be found under https://doi.org/10.1002/adfm.202000642.

Dr. Y. Deng
Core Research Facilities
Southern University of Science and Technology
Shenzhen 518055, China

Prof. X. Cheng
Department of Materials Science and Engineering
South University of Science and Technology of China
No. 1088, Xueyuan Road, Shenzhen, Guangdong 518055, China

Prof. D. Lei
Department of Materials Science and Engineering
City University of Hong Kong
83 Tat Chee Avenue, Kowloon, Hong Kong, China
E-mail: dangylei@cityu.edu.hk

Prof. Y. Deng
State Key Laboratory of Applied Optics
Changchun Institute of Optics
Fine Mechanics and Physics (CIOMP)
Chinese Academy of Sciences
Changchun 130033, China
E-mail: dengyb@ciomp.ac.cn

DOI: 10.1002/adfm.202000642

clusters are generally orders of magnitude larger due to the strong capacitive coupling of surface plasmons oscillating in adjacent nanoparticles.[21,22] Therefore, plasmonic nanodimers and nanoclusters with nanometer-sized vacuum or dielectric gaps have become a versatile plasmonic nanocavity platform for a variety of fundamental studies and prototype applications ranging from quantum plasmonics to plasmon-induced photochemistry.[23–25] On the one hand, the rapid progress in advancing the resolution of nanofabrication techniques enables the field enhancement to be further increased by shrinking gap sizes. However, the challenge of fabricating plasmonic nanogaps at the sub-10-nm scale by the existing nanofabrication techniques has exhausted the increment of field enhancement through solely narrowing the gap sizes.[26,27] On the other hand, the geometric optimization to concentrate surface charges in plasmonic hotspots and suppress the decay of plasmon resonance has been exploited to leverage the near-field enhancement in plasmonic nanostructures. For example, the "lightening rod effect"-based bowtie nanodimer design presented larger electric field enhancement factor than that in disk nanodimers.[28,29] In the framework of shape optimization, gold nanorods exhibited drastic reduction of plasmon damping as compared to small nanospheres due to suppressed interband damping, implying larger local field enhancement factors and higher light-scattering efficiencies.[30] Furthermore, delicate geometry design of fan-shaped gold nano-antennas integrating the geometric advantages of both bowtie and rod shapes resulted in the maximal near-field enhancement among the reported plasmonic nanodimers due to the suppression of radiation loss and larger charge reservoir in the circular ends.[31] Nevertheless, the above-mentioned strategies to maximize near-field enhancement factors have been mostly based on shape and size optimizations of simple particle geometries. The limited exploration of new designs and the present time-consuming full-wave based optimization methods tend to omit the optimal solutions. Therefore, seeking efficient optimization paths and exploring optimal geometry designs may pave the way for achieving maximal possible plasmonic field enhancement.

Topology optimization-based inverse design is well advised to observe certain details in the boundary conditions of desired patterns and target functions.[32] For the given functionality of maximal field enhancement, topology optimization can be used to retrieve the geometric parameters of plasmonic nanostructures to solve the inverse problem.[33–35] Herein, we implement a topology optimization algorithm to inversely design gold nanoparticle dimers with sub-10-nm gap sizes driven by the desired functionality of maximizing near-field enhancement factors in the gaps. The solution of inverse problem is analyzed using the continuous adjoint method to derive the gradient information of the design objective and solved by an iterative approach.[36,37] Based on the adjoint analysis, the iterative solution process converges efficiently, and the result in convergence is highly independent of the initial structure. Applying the topology optimization algorithm gives rise to a gold nanodimer of heart-shaped nanoparticles, which exhibits a substantially larger near-field enhancement factor in the gap than gold nanodimers of either rod- or triangle- and disk-shaped nanoparticles and the same gap size. Full-wave electromagnetic (EM) analysis reveals the heart-shaped nanostructure dimer possesses the highest concentration of surface charges at the particle apex compared to the other shapes. Moreover, we utilize the state-of-the-art focused helium ion beam milling (He^+-FIB) technique combined with our recently developed "sketch and peel" strategy to achieve the high-fidelity fabrication of heart-, bowtie-, and disk-shaped nanoparticle dimers with an ultrasmall gap size of 5 nm.[38] Finally, their near-field enhancement performances are experimentally characterized with nonlinear optical spectroscopies at the single-particle level. The signal intensities of surface-enhanced Raman spectroscopy (SERS) and two-photon photoluminescence (TPPL) of the heart-shaped nanoparticle dimer are much stronger than those of the other two structures, verifying the validity and effectiveness of the topology optimization-based inverse design of plasmonic nanostructures with desired functionalities.

2. Results and Discussion

2.1. Topology Optimization

The topology optimization procedure in the present work is sketched in **Figure 1**. The topology optimization focuses on materials distribution and geometric configuration of plasmonic nanostructures possessing maximal field enhancement factors at the desired position.[33,35] As demonstrated from the 3D schematics of Figure 1a, the characteristics of structure can be indicated by the enhancement of electric field in hotspots when an EM wave illuminates onto the periodic plasmonic nanostructures. For the variational problem of periodic structures, it can be simplified as the single structure in the unit cell (labeled by the dashed-line box in the bottom panel of Figure 1a) of optimization problem with periodic boundary conditions in both x and y directions. To maintain the electric neutrality of the metallic nanostructure, the divergence free condition is imposed on the electric field in the computational domain, and the target function of near-field enhancement factor at the specified position can be described as:

$$\Phi(E_s)=\left[\frac{(E_s+E_i)\cdot(\overline{E}_s+\overline{E}_i)}{E_i\cdot\overline{E}_i}\right]^2\Bigg|_{x=x_0}=\int_\Omega\left[\frac{(E_s+E_i)\cdot(\overline{E}_s+\overline{E}_i)}{E_i\cdot\overline{E}_i}\right]^2\cdot\delta(x-x_0)\cdot d\Omega \tag{1}$$

where the electric field E is divided into two components, i.e., the scattered field E_s and the incident field E_i; x_0 is the location of the hotspot interested; $x=(x, y, z)^T$ is the space coordinate; $\delta(x-x_0)$ is the Dirac function; Ω is the computational domain. In the inverse design procedure, the scattering of EM wave in the near-field of plasmonic nanostructure array is described by the wave equation based on the reduction of Maxwell's equations:

$$\nabla\times\left[\mu_r^{-1}\nabla\times(E_s+E_i)\right]-k_0^2\varepsilon_r(E_s+E_i)=0, \text{ in } \Omega \tag{2}$$

where the time dependence factor is set to be $e^{j\omega t}$, j, ω, and t respectively represent the imaginary unit, the angular frequency, and the time; ε_r and μ_r are the relative electric permittivity and magnetic permeability, respectively. $k_0=\omega\sqrt{\varepsilon_0\mu_0}$ is

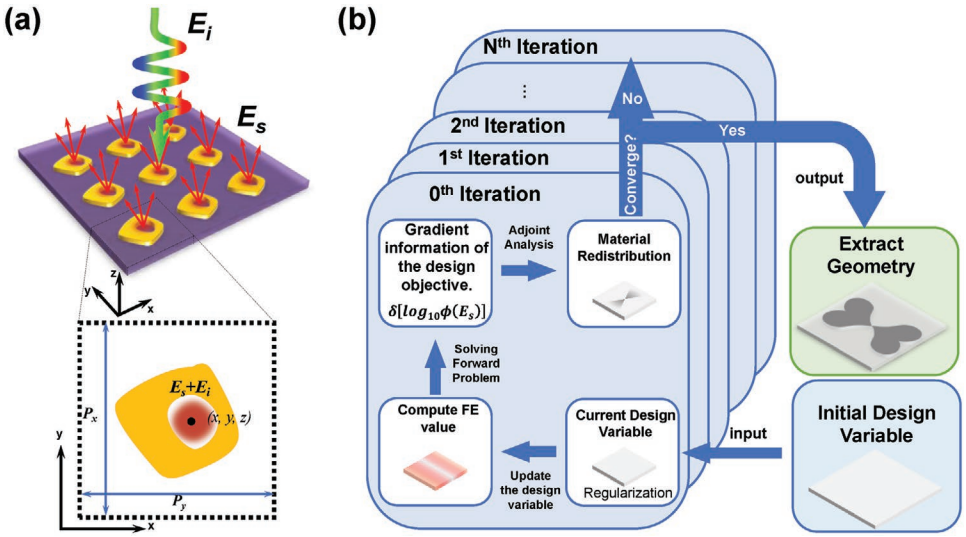

Figure 1. Sketched scheme of inverse design of a plasmonic nanostructure array to maximize near-field enhancement. a) The 3D model of localized surface plasmon resonance in periodic gold nanostructures. The inset sketches a zoomed-in structure of design domain. b) The structure of the topology optimization algorithm used in our work.

the wave number in free space, with electric permittivity ε_0 and magnetic permeability μ_0. The parameter Ω presents the computational domain for the nanostructures (see the details of optimization procedure in Supporting Information). The optimization procedure is based on the material interpolation where two material phases are related by the material density.[33] A simple optimization procedure is shown in Figure 1b. As the procedure starts, the initial condition is a homogeneous distribution of vacuum in design domain. In the first iteration, the input material density is related with a design variable valued in [0, 1] unlike binary in evolutionary optimization and regularized by density filter and projection to remove the grayscale pixels that presents the middle status between two different materials.[39–41]

The field enhancement of structure with the input of material density is calculated by solving forward problem. The variational problem after forward solution is analyzed by using the continuous adjoint method to derive the gradient information of the design. Then, the optimization problem is solved by using an iterative approach. Finally, the optimization procedure will judge the convergence of calculation in each iteration based on the preset tolerance. If not convergence, the optimization loop is followed with those sequential steps till the difference of objective value between two adjacent iterations below the convergence criteria.

In this work, we regularize the configuration of plasmonic nanodimers in design domain, because the plasmonic dimers enable most of the incident light energy to be focused in the single nanogap. Therefore, the performance of plasmonic dimers is evaluated by the enhancement factor of electric field in the gaps. As schematically shown in **Figure 2**a, the basic configuration of dimer consists of two mirror Au nanostructures with a 10-nm gap in between on the quartz substrate. Subject to the fabrication method based on planar process, the piecewise homogeneous assumption is acceptable for the material filled in design domain (500 × 500 nm). The material interpolation in computational domain is related with the design variable valued in [0, 1], where "0" and "1" represent vacuum and gold (Au), respectively. During the iterative procedure, the initial homogeneous distribution transits to the dielectric continuum and converges to the dielectric constant of Au or vacuum over the evolution of 170 iterations, as plotted in Figure 2b. Meanwhile, the enhancement factor ($[|E/E_{inc}|]^4$) in gaps soars up from initial condition to 10th iteration and then gradually converges to the platform at the maximal enhancement factor around 2.7×10^7. Therefore, the geometry from the design variable is extracted. Interestingly, the resultant geometry is a heart-shaped nanoparticle dimer with the tip-to-tip arrangement. As a quick test of the validity of the result, the performance of field enhancement of commonly used structures is also examined briefly via finite element method (FEM) simulation. As shown in Figure 2c, the enhancement factor in the gap of heart-shaped dimer is much larger than that of rod-, bowtie-, and disk-shaped nanoparticle dimers, which is due to the combination of concave/convex feature in heart-shaped geometry that would help the optimization of field enhancement.[42]

The physical origin of the maximal field enhancement in the inversely designed heart-shaped nanoparticle dimer is analyzed from the perspective of surface charge localization, and the results are shown in **Figure 3**. As described by Maxwell's equations, the intensity of electric field is the division of charges. For the dimer configuration, the large enhancement of electric field in the near field of nanogap is ascribed to the strong capacitive coupling of the highly concentrated oscillated charges in the opposite sides of nanogap. In Figure 3a, the plot of maximal charge density in the iterative nanoparticle dimers illustrates that the raising of charge density contributes the achievement of maximal field enhancement in the gap. The iterative trend of maximal charge density is agreement with that of near-field enhancement in Figure 2b. In Figure 3b, the charge distribution from five representative results in the evolution of iterations presents that the charge density of two opposite apexes of nanoparticle

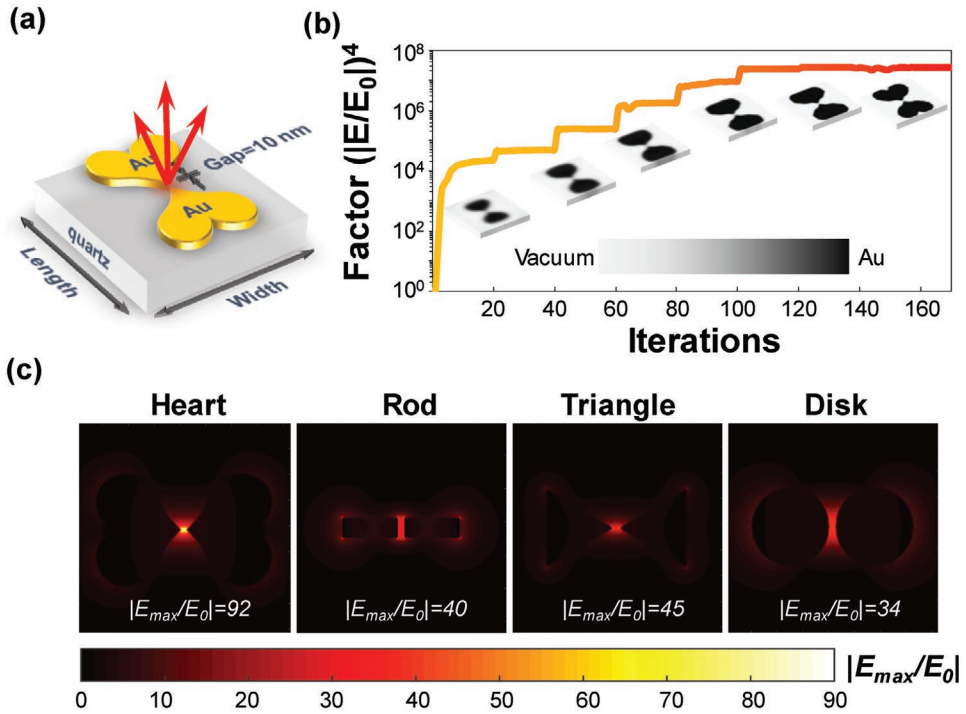

Figure 2. Overview of inverse design driven by the functionality of maximizing near-field enhancement. a) The 3D model of gold nanoparticle dimer with predefined key parameters in geometry and material. b) The enhancement factor of electric-field in the nanodimer gap over the evolution of multiple iterations. The data of near-field enhancement factors are from the calculation results using the FEM algorithm. c) The electric-field distribution of heart-, rod-, triangle-, and disk-shaped nanoparticle dimers. All the near-field mappings are simulated by the FEM approach. The four kinds of dimeric nanostructures have similar resonant energy at the wavelength of 800 nm (see Figure S1, Supporting Information).

in gaps increases with the iterative evolution of geometry and maximizes at the convergence of optimization algorithm. The resultant heart-shaped nanoparticle dimer not only exhibits the best performance of near field enhancement at the specific wavelength set in the topology optimization algorithm, but also performs as the superior design in structure geometry in the

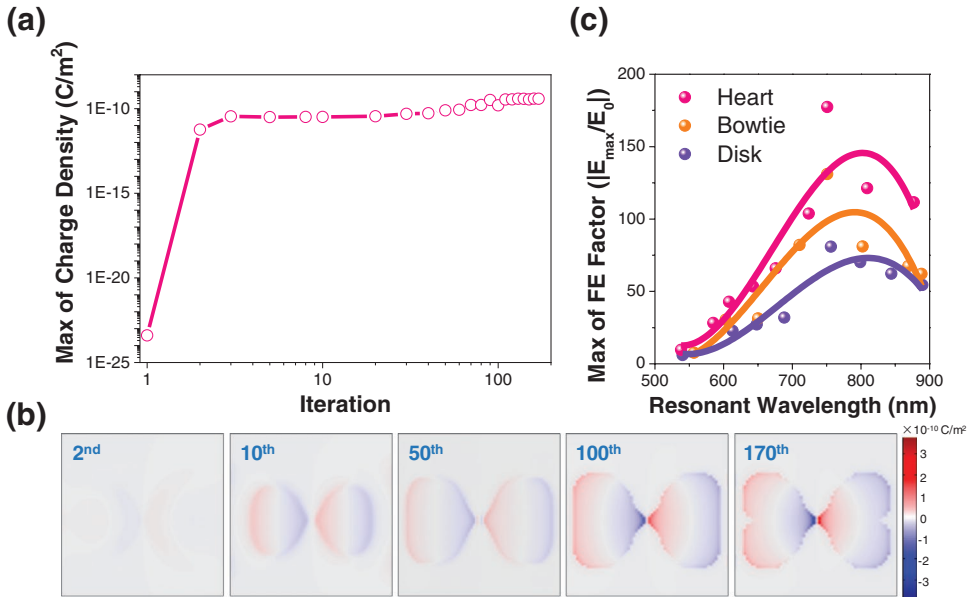

Figure 3. The analysis of maximal field enhancement on heart-shaped dimer. a) The maximal charge density as a function of iterations in optimization process. The data of charge density is from the calculation of FEM simulations. b) The charge distribution of some representative dimer nanostructures in the iterative optimization process. The data are extracted from the iterative results in calculation using FEM algorithm. c) The calculated maximal field enhancement as a function of resonant wavelength of proportional different-shape dimers with scaling up and down. The data in this plot are calculated based on FEM algorithm. The three solid lines are overlaid on the simulated data points to qualitatively show the evolution trend of corresponding data points. All dimers in simulation mode were set to the same gap size of 10 nm.

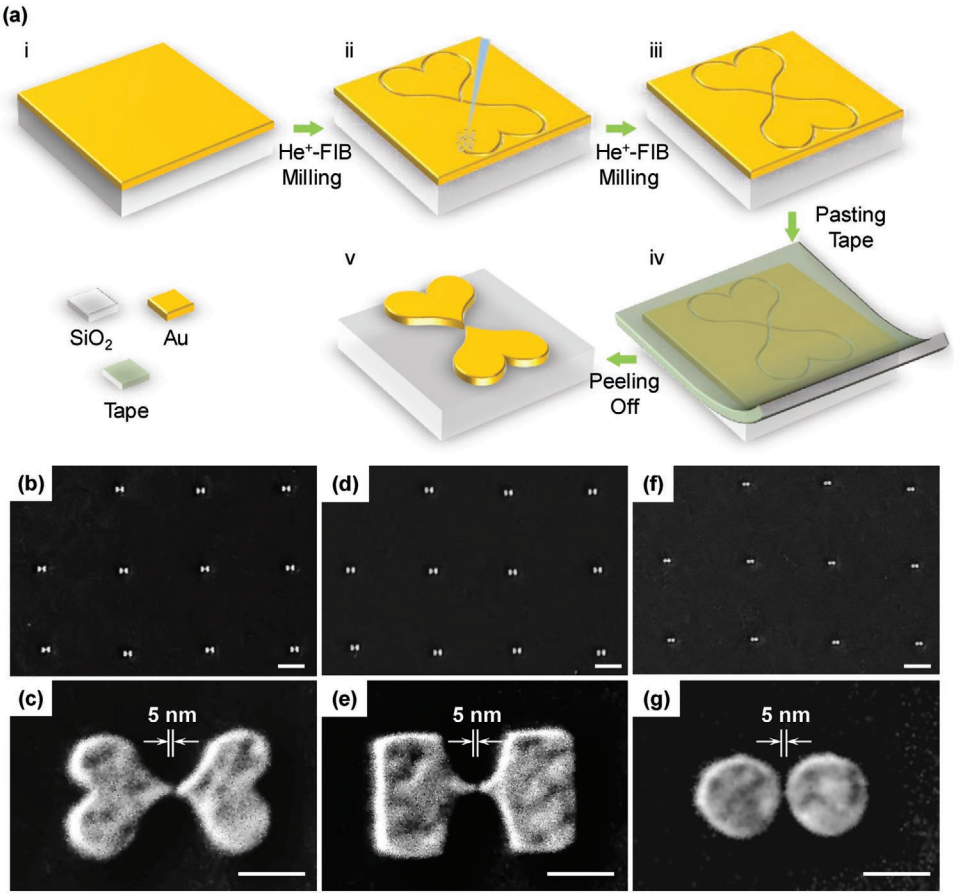

Figure 4. The fabrication methodology and the gallery of three kinds of Au nanoparticle dimers with different shapes. a) The flowing charts of fabrication method to define heart-shaped nanoparticle dimer by He^+-FIB milling using the "sketch and peel" strategy. b,d,f) The SEM images of arrayed Au nanoparticle dimers with different shapes. c,e,g) The corresponding high-resolution electron micrographs of single nanodimer. b,c) Heart-shaped; d,e) bowtie-shaped; f,g) disk-shaped nanoparticle dimer. Scale bars: 1 µm in (b),(d), and (f); 100 nm in (c),(e), and (g).

broad range of resonant wavelength from 550 to 900 nm compared to heart-, rod-, triangle-, and disk-shaped nanoparticle dimers. As shown in Figure 3c, the serial proportional heart-shaped nanoparticle dimers indicate a higher factor of near-field enhancement than that performed in the control disk- and bowtie-shaped nanoparticle dimer series in the case of the same resonant wavelength at a wide range of resonant wavelength.

2.2. Nanostructure Fabrication

The 10-nm gap and the complexity of geometry in heart-shaped nanodimer are indeed the extreme challenge for nanofabrication techniques in the perspective of resolution and accuracy.[43] Here, we reliably fabricate the optimized gold heart-shaped nanoparticle dimer using the state-of-the-art nanofabrication technique we developed previously. This technique is based on an ultrahigh-resolution He^+-FIB milling process with the advanced "sketch and peel" strategy,[38] as shown in **Figure 4**a. First, the nanopatterning of heart-shaped nanoparticle dimer was carried out on a 30-nm-thickness gold film supported by a quartz substrate. The Au film was patterned to be the ultra-narrow outline slit of heart-shaped dimer by He^+-FIB milling. To define sub-10-nm gap, we designed the gap region in layout using a shared boundary.[44] A tape-stripping can selectively peel off the outside film and remain the inside target structure on the substrate. In our previous work, direct patterning outline using FIB process combined with "sketch and peel" strategy has demonstrated the tremendous improvement of the resolution and accuracy of fabricated nanostructures. The SEM images in Figure 4b present the resultant Au heart-shaped dimer array with no defects. The enlarged electron micrograph of single heart-shaped nanoparticle dimer in Figure 4c shows the 5-nm resolution of gap fabrication and the sub-5-nm accuracy in the definition of convex and concave nanofeatures. Meanwhile, we also fabricated the bowtie-shaped (the intermediate result in optimization, in Figure 4d,e) and disk-shaped nanoparticle dimers (the conventional design, in Figure 4f,g) which possess the similar gap size with that of heart-shaped nanoparticle dimer for comparison.

2.3. Nonlinear Optical Spectroscopy

Enhancing optical nonlinear processes is a significant application in plasmonics. The enhancement factor of nonlinear

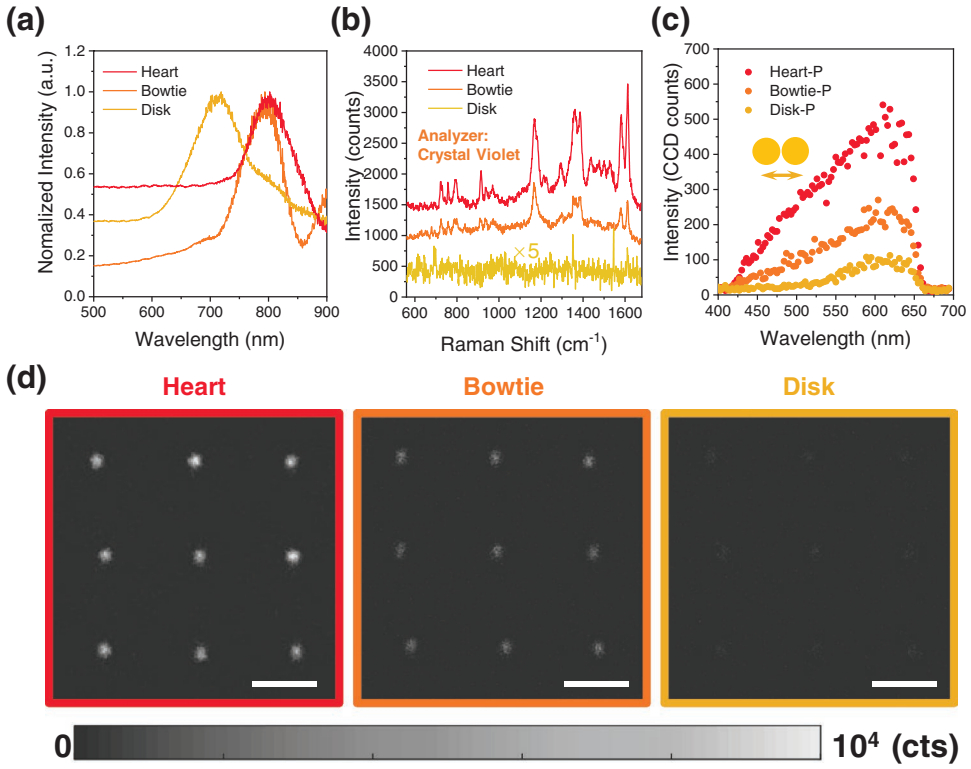

Figure 5. The SERS and TPPL nonlinear applications. a) Single-particle dark-field scattering spectra of three kinds of nanoparticle dimers with different shapes. b) The measurement of SERS spectra of three kind of nanoparticle dimer. Here each Raman spectrum is an averaged curve of five spectra measured for five individual dimers in the same array (see the original Raman spectra in Figure S3, Supporting Information). The Raman probe molecule used in this study is crystal violet molecule. c) The TPPL characterization of heart-shaped (red dot), bowtie-shaped (orange dot), disk-shaped (yellow dot) dimers at the polarized excitation of 800 nm along the gapped direction. d) The corresponding mapping of three kinds of dimers with the integration of signals at the range of 400–650 nm. The color bar represents the intensity of integrated TPPL signals in the mapping pictures. Scale bar is 2 μm.

effect is strongly dependent on the localized intensity in the high-field region of plasmonic structures. In **Figure 5**, SERS and TPPL of plasmonic structure were carried out to evaluate the performance of field enhancement around gold nanoparticle dimers in Figure 4. Before this evaluation, the resonant energy of optimized heart-shaped nanoparticle dimer and other two kinds of dimers were characterized using dark-field scattering. In Figure 5a, the resonant energy of both heart-shaped dimer and bowtie-shaped nanoparticle dimer at the wavelength of 800 nm precisely matches with the excitation energy (785 nm) in our optimization model. As a comparison, the disk-shaped nanoparticle dimer presents a scattering peak at a spectral location of 700 nm. The energy match and mismatch between resonant and excitation wavelength in SERS application exhibit the on-resonance and off-resonance enhancement when choosing the excitation wavelength of 785 nm, a widely used EM wave in SERS measurement. In Figure 5b, the heart-shaped and bowtie-shaped nanoparticle dimers under on-resonance condition perform the appreciable amplification of Raman signal from analyzer with the magnitude of over 10 times compared to that the disk dimer does. Meanwhile, the enhancement factor of heart-shaped nanoparticle dimer is higher than that of bowtie-shaped dimer, which illustrates the largest near-field enhancement in heart-shaped dimer. In contrast, the Raman enhancement is switched off when the incident laser polarization changes to be perpendicular to the axis of each dimer (see Figure S2, Supporting Information).

Similar to the SERS-based near-field enhancement characterization, two-photon photoluminescence spectroscopy is also an effective means to reveal the local near-field enhancement factors in plasmonic hotspots. The measurements of TPPL intensities for the three types of gold nanoparticle dimers were carried out to evaluate their respective near-field enhancement. Figure 5c shows the TPPL spectra for the three structures. Obviously, under an on-resonance excitation at 800 nm, the heart- and bowtie-shaped nanoparticle dimers exhibit substantially higher signal intensities than that of the disk-shaped nanoparticle dimer under an off-resonance excitation. Meanwhile, the signal intensity of the heart-shaped nanoparticle dimer is the highest among the three kinds of dimeric structures because of the combination of its greatest capability of near-field enhancement and higher optical state under the on-resonance excitation condition. The spectral dependence of TPPL signal intensities for the three kinds of nanoparticle dimers are also consistent with the calculated near-field enhancement factors shown in Figure 3c. These results in Figure 5c also verify the robust effectiveness of the topology optimization algorithm with the functionality of maximizing near-field enhancement. Furthermore, the uniform signal mapping on each squared area containing

3 × 3 nanoparticle dimers shown in Figure 5d illustrates that our fabrication method possesses precise control over gap size at the sub-10-nm scale. We observe that the intensity brightness of periodic dots in the 2D mappings gradually decreases from the heart- to disk-shaped nanoparticle dimer, which agrees well with the spectral intensity measurements in Figure 5c.

3. Conclusions

In summary, the topology optimization algorithm driven by the desired functionality of maximizing near-field enhancement factor in the gaps is proposed, leading to the discovery of the heart-shaped nanoparticle dimer with sub-10-nm gap. By employing full-wave EM analysis, the heart-shaped nanoparticle dimer demonstrates the best near-field enhancement compared to the bowtie- and disk-shaped nanoparticle dimer based on simple geometries in design. The new developed method combining He^+-FIB milling with "sketch and peel" strategy ensures the reliable fabrication of the optimized heart-, control bowtie-, and disk-shaped nanoparticle dimer with uniform defined gap distances down to 5 nm. The SERS and TPPL nonlinear optical spectroscopies of these nanoparticle dimers demonstrated that the heart-shaped nanoparticle dimer exhibits the highest signal intensities when compared with those in the other two dimers. The results also corroborate the validity and effectiveness of inverse design of plasmonic nanostructures with the desired functionalities based on topology optimization. Hence, the inverse design is an effective approach to further boost the optimal performance of plasmonic devices toward specific functionalities and applications.

4. Experimental Section

Fabrication: The fabrication of sample was performed on a pure gold film with a thickness of 30 nm using a helium ion microscopy (ZEISS ORION NanoFab). The complex layout of heart-shaped and dumbbell-shaped dimer was extracted from the geometry in optimization procedure. We sketched the outline of pixelated pattern with the spline curve. The outline was separated into two parts, gap region and the rest part in layout. To reduce the redeposition effect, we executed the recirculated milling. The two separated outline parts help us to independently tune the ion dose for defining high-resolution nanogap in dimers. After He^+-FIB milling, we pasted a Scotch tape onto the surface of as-fabricated gold film and used a tweezer to catch one side of tape and peel it off. Finally, only the target gold nanostructures remained on substrate.

SERS Measurement: The SERS measurement was characterized on a confocal Raman microscopy (Renishaw inVia) system. To prepare the sample for Raman enhancement, the substrate supporting gold nanoparticles was immersed into the ethanol solution of crystal violet (CV) with the concentration of 5×10^{-5} M for 24 h and rinsed by ethanol to confirm a monolayer of molecules on the surface of nanoparticle. Finally, the sample was dried by a steady blowing of nitrogen gas. In the measurement, the excitation laser of 785 nm was introduced into the confocal microscope and focused onto the nanoparticle by a 100 × objective (NA = 0.85). The linear polarization of laser was parallel with the gapped axis. The power of excitation energy was set to be 850 μW and the signal was extracted with an integration time of 2 s for three times.

Dark-Field Scattering Characterization: During the measurement, the incident light from halogen lamp (315° K, 100 W) through the dark-field module excited the particle with the glancing of annular illumination. The scattering signal was collected by a 50 × objective (ZEISS Epiplan, NA = 0.75). In the collection path, the pinhole excluded the noise signals from the surrounding area of single measured nanoparticles. Meanwhile, the piezoelectric stage was used to guarantee the measured nanoparticle located in the region of focal spot. The signal was detected by an electric-cooled CCD camera (Andor DV 401A-BV-352). The signal was extracted with an integration time of 10 s for five times. The calculation of normalized scattering intensity is performed using the equation as follows:

$$I_{\text{scat}}(\lambda) = \frac{I_{\text{particle}} - I_{\text{sub}}}{I_{\text{source}} - I_{\text{dark}}} \tag{3}$$

where $I_{\text{scat}}(\lambda)$ is the real scattering signal from a single gold nanostructure; the spectrum of I_{particle}, I_{sub} is separately measured from the original particle and the adjacent substrate. I_{source} and I_{dark} are the spectrum of the light source and the background count of the measurement system, respectively.

Two-Photon Photoluminescence Spectroscopy: The characterization of two-photon photoluminescence was used by the Leica SP8 MP system. The wavelength of the fs-laser was 800 nm with the power density of 1.1×10^8 W m^{-2}. Total scanning time of one single structure from 394 to 694 nm was around 5.53 s, and the exposure time of signal extraction from single structure in each pixel was set to about 0.05 s.

EM Simulation: The field enhancement in control was calculated based on the FEM algorithm using commercial software COMSOL Multiphysics. The modeling of inversely design heart-shape and case-shape dimer in geometry was based on the coordination data extracted from optimization procedure. In this work, the dielectric constant of gold used in our simulation was from the Johnson & Christy database in the reference in simulation,[45] and indeed our EM wave calculations did not incorporate the size effect of gold permittivity in the tip regions of the designed dimers, that is, the classic local response of gold is considered in our EM wave analysis. In general, spatial nonlocality and thickness-dependent permittivity of metal could be negligible for the length scales of height (30 nm) and gap (5 nm) for the dimers experimentally prepared in this study, as already demonstrated in previous studies.[27,46,47] Meanwhile, previous studies have experimentally demonstrated that the classical electrodynamics still holds true when the tip size of gold nanobowties or the gap distance between gold nanospheres and a gold film is above ≈1 nm.[27,48]

Supporting Information

Supporting Information is available from the Wiley Online Library or from the author.

Acknowledgements

Y.C. and Y.H. contributed equally to this work. The authors are grateful to Dr. Shaoding Liu in Taiyuan University of Technology and Dr. Xupeng Zhu in Lingnan Normal University for helpful discussions. This work was supported by the National Natural Science Foundation of China (Grants Nos. 51722503, 51621004, 51805160, 11574078, and 51875545), the Hong Kong Research Grants Council (GRF Project No. 15303417), and the open fund of State Key Laboratory of Applied Optics.

Conflict of Interest

The authors declare no conflict of interest.

Keywords

inverse design, near-field enhancement, nonlinear optics, plasmonic nanostructures, topology optimization

Received: January 22, 2020
Revised: March 15, 2020
Published online: April 8, 2020

[1] E. Fort, S. Grésillon, *J. Phys. D: Appl. Phys.* **2008**, *41*, 013001.
[2] A. Kinkhabwala, Z. Yu, S. Fan, Y. Avlasevich, K. Müllen, W. E. Moerner, *Nat. Photonics* **2009**, *3*, 654.
[3] N. E. Hecker, R. A. Höpfel, N. Sawaki, T. Maier, G. Strasser, *Appl. Phys. Lett.* **1999**, *75*, 1577.
[4] K. Okamoto, I. Niki, A. Shvartser, Y. Narukawa, T. Mukai, A. Scherer, *Nat. Mater.* **2004**, *3*, 601.
[5] R. Jiang, B. Li, C. Fang, J. Wang, *Adv. Mater.* **2014**, *26*, 5274.
[6] S. Nie, S. R. Emory, *Science* **1997**, *275*, 1102.
[7] K. Kneipp, Y. Wang, H. Kneipp, L. T. Perelman, I. Itzkan, R. R. Dasari, M. S. Feld, *Phys. Rev. Lett.* **1997**, *78*, 1667.
[8] H. Xu, E. J. Bjerneld, M. Käll, L. Börjesson, *Phys. Rev. Lett.* **1999**, *83*, 4357.
[9] M. Kauranen, A. V. Zayats, *Nat. Photonics* **2012**, *6*, 737.
[10] C. Chen, A. R. B. de Castro, Y. Shen, *Phys. Rev. Lett.* **1981**, *46*, 145.
[11] M. Sivis, M. Duwe, B. Abel, C. Ropers, *Nat. Phys.* **2013**, *9*, 304.
[12] S. Kim, J. Jin, Y.-J. Kim, I.-Y. Park, Y. Kim, S.-W. Kim, *Nature* **2008**, *453*, 757.
[13] C. Clavero, *Nat. Photonics* **2014**, *8*, 95.
[14] Y. Kang, S. Najmaei, Z. Liu, Y. Bao, Y. Wang, X. Zhu, N. J. Halas, P. Nordlander, P. M. Ajayan, J. Lou, Z. Fang, *Adv. Mater.* **2014**, *26*, 6467.
[15] Z. Fang, Y. Wang, Z. Liu, A. Schlather, P. M. Ajayan, F. H. L. Koppens, P. Nordlander, N. J. Halas, *ACS Nano* **2012**, *6*, 10222.
[16] M. W. Knight, H. Sobhani, P. Nordlander, N. J. Halas, *Science* **2011**, *332*, 702.
[17] Y. Liu, R. Cheng, L. Liao, H. Zhou, J. Bai, G. Liu, L. Liu, Y. Huang, X. Duan, *Nat. Commun.* **2011**, *2*, 579.
[18] Y. Hu, H. Wu, Y. Meng, D. B. Bogy, *J. Appl. Phys.* **2017**, *122*, 134303.
[19] Y. Hu, H. Wu, Y. Meng, Y. Wang, D. Bogy, *J. Appl. Phys.* **2018**, *123*, 034303.
[20] L. Pan, D. B. Bogy, *Nat. Photonics* **2009**, *3*, 189.
[21] M. Hentschel, M. Saliba, R. Vogelgesang, H. Giessen, A. P. Alivisatos, N. Liu, *Nano Lett.* **2010**, *10*, 2721.
[22] N. Pazos-Perez, C. S. Wagner, J. M. Romo-Herrera, L. M. Liz-Marzán, F. J. García de Abajo, A. Wittemann, A. Fery, R. A. Alvarez-Puebla, *Angew. Chem., Int. Ed.* **2012**, *51*, 12688.
[23] G.-C. Li, Q. Zhang, A. Maier Stefan, D. Lei, *Nanophotonics* **2018**, *7*, 1865.
[24] J. J. Baumberg, J. Aizpurua, M. H. Mikkelsen, D. R. Smith, *Nat. Mater.* **2019**, *18*, 668.
[25] B. Luk'yanchuk, N. I. Zheludev, S. A. Maier, N. J. Halas, P. Nordlander, H. Giessen, C. T. Chong, *Nat. Mater.* **2010**, *9*, 707.
[26] J. Zuloaga, E. Prodan, P. Nordlander, *Nano Lett.* **2009**, *9*, 887.
[27] H. Duan, A. I. Fernández-Domínguez, M. Bosman, S. A. Maier, J. K. W. Yang, *Nano Lett.* **2012**, *12*, 1683.
[28] A. V. Ermushev, B. V. McHedlishvili, V. A. Oleĭnikov, A. V. Petukhov, *Quantum Electron.* **1993**, *23*, 435.
[29] J. P. Kottmann, O. J. F. Martin, D. R. Smith, S. Schultz, *Chem. Phys. Lett.* **2001**, *341*, 1.
[30] C. Sönnichsen, T. Franzl, T. Wilk, G. von Plessen, J. Feldmann, O. Wilson, P. Mulvaney, *Phys. Rev. Lett.* **2002**, *88*, 077402.
[31] L. V. Brown, X. Yang, K. Zhao, B. Y. Zheng, P. Nordlander, N. J. Halas, *Nano Lett.* **2015**, *15*, 1272.
[32] M. Bendøse, O. Sigmund, *Topology Optimization: Theory, Methods, and Applications*, Springer-Verlag, Heidelberg, Germany **2003**.
[33] Y. Deng, Z. Liu, C. Song, P. Hao, Y. Wu, Y. Liu, J. G. Korvink, *Struct. Multidiscip. Optim.* **2016**, *53*, 967.
[34] E. Wadbro, C. Engström, *Comput. Methods Appl. Mech. Eng.* **2015**, *293*, 155.
[35] R. E. Christiansen, J. Vester-Petersen, S. P. Madsen, O. Sigmund, *Comput. Methods Appl. Mech. Eng.* **2019**, *343*, 23.
[36] Y. Deng, J. G. Korvink, *J. Comput. Phys.* **2018**, *370*, 85.
[37] P. Hansen, L. Hesselink, *Opt. Express* **2015**, *23*, 23899.
[38] Y. Chen, K. Bi, Q. Wang, M. Zheng, Q. Liu, Y. Han, J. Yang, S. Chang, G. Zhang, H. Duan, *ACS Nano* **2016**, *10*, 11228.
[39] B. S. Lazarov, O. Sigmund, *Int. J. Numer. Mech. Methods Eng.* **2011**, *86*, 765.
[40] J. K. Guest, J. H. Prévost, T. Belytschko, *Int. J. Numer. Mech. Methods Eng.* **2004**, *61*, 238.
[41] T. Feichtner, O. Selig, M. Kiunke, B. Hecht, *Phys. Rev. Lett.* **2012**, *109*, 127701.
[42] A. García-Etxarri, P. Apell, M. Käll, J. Aizpurua, *Opt. Express* **2012**, *20*, 25201.
[43] F. Fang, N. Zhang, D. Guo, K. Ehmann, B. Cheung, K. Liu, K. Yamamura, *Int. J. Extrem. Manuf.* **2019**, *1*, 012001.
[44] Y. Chen, Q. Xiang, Z. Li, Y. Wang, Y. Meng, H. Duan, *Nano Lett.* **2016**, *16*, 3253.
[45] P. B. Johnson, R. W. Christy, *Phys. Rev. B* **1972**, *6*, 4370.
[46] S. Laref, J. Cao, A. Asaduzzaman, K. Runge, P. Deymier, R. W. Ziolkowski, M. Miyawaki, K. Muralidharan, *Opt. Express* **2013**, *21*, 11827.
[47] Q. Zhang, X. Cai, X. Yu, S. Carregal-Romero, W. J. Parak, R. Sachan, Y. Cai, N. Wang, Y. Zhu, D. Y. Lei, *Adv. Quantum Technol.* **2018**, *1*, 1800016.
[48] D. Liu, T. Wu, Q. Zhang, X. Wang, X. Guo, Y. Su, Y. Zhu, M. Shao, H. Chen, Y. Luo, D. Lei, *ACS Nano* **2019**, *13*, 7644.